Itinerant Half-Metal Spin-Density-Wave State on the Hexagonal Lattice

Rahul Nandkishore,[1] Gia-Wei Chern,[2] and Andrey V. Chubukov[2]
[1]Department of Physics, Massachusetts Institute of Technology, Cambridge, Massachusetts 02139, USA
[2]Department of Physics, University of Wisconsin-Madison, Madison, Wisconsin 53706, USA
(Received 9 February 2012; published 30 May 2012)

We consider electrons on a honeycomb or triangular lattice doped to the saddle point of the band structure. We assume the system parameters are such that spin density wave (SDW) order emerges below a temperature T_N and investigate the nature of the SDW phase. We argue that at $T \leq T_N$, the system develops a uniaxial SDW phase whose ordering pattern breaks $O(3) \times Z_4$ symmetry and corresponds to an eight-site unit cell with nonuniform spin moments on different sites. This state is a half-metal—it preserves the full original Fermi surface, but has gapless charged excitations in one spin branch only. It allows for electrical control of spin currents and is desirable for nanoscience.

DOI: 10.1103/PhysRevLett.108.227204 PACS numbers: 75.10.Lp, 73.22.Pr, 75.30.Fv

Introduction.—The electronic properties of single-layer graphene have been the subject of considerable experimental and theoretical interest [1]. Near half-filling, a description in terms of noninteracting Dirac electrons captures the essential physics, since interactions effects are suppressed by the low density of states (DOS). A sharply different behavior arises when graphene is strongly doped to $3/8$ or $5/8$ filling [2]. At this filling, a divergent density of states and nested Fermi surface (FS) conspire to produce weak coupling instabilities to an extensive buffet of ordered states, including spin density waves (SDW) [3–5], Pomeranchuk metals [6], and d wave superconductors (SC) [7–9]. A similar situation arises on a triangular lattice at $3/4$ filling [10,11].

It has recently been established using renormalization group (RG) methods [7] that the two most relevant instabilities at weak coupling are toward SDW and a d-wave SC. Other potential instabilities, like a charge-density wave, have much smaller susceptibilities. The SDW vertex is the largest at intermediate RG scales, but superconducting vertex eventually overshoots it, making d-wave superconductivity the leading weak coupling instability at the van Hove filling. The SC state has a $d + id$ gap structure and breaks time-reversal symmetry [7]. Upon doping away from van Hove filling, the Cooper and SDW channels decouple at a scale set by doping, and the RG flow is altered. In this situation, the SDW, which is the largest at intermediate RG scales, may become the dominant instability, and numerical functional RG studies found [8] that SDW is indeed the leading instability in substantially wide doping range away from $3/8$ or $5/8$. Previous work on SDW order argued that the SDW state is noncoplanar and has nonzero spin chirality [3,5,10]. Such a state gaps out the entire Fermi surface (FS).

We argue that the situation is more complex than originally thought, and the chiral SDW state is present only at the lowest temperatures. Over a wide intermediate range of temperatures, a different SDW state emerges in which SDW order develops simultaneously at three inequivalent wave vectors $\mathbf{Q}_i$, but the three vector order parameters are all aligned along the same axis. This state has an eight-site unit cell with nonuniform spin moments and zero net magnetization [Fig. 1(b)]. Such a state cannot be accessed starting from a spin Hamiltonian for local moments with a fixed length and can only be accessed starting from a model of itinerant fermions. We show that in this state, unlike in any other known SDW state, the chemical potential shifts proportionally to the SDW order parameter, preserving the original Fermi surface for one spin branch and gapping out the other spin branch. The uniaxial SDW state is therefore a ''half-metal'' that allows for electrical control of spin currents. Such a state is highly desirable for nanoscience applications.

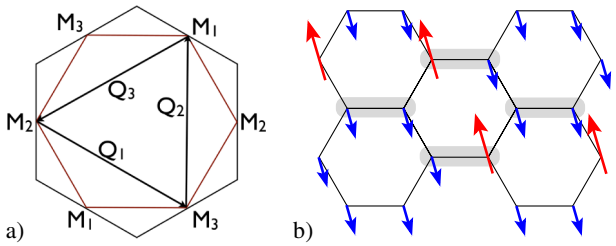

FIG. 1 (color online). (a) The Fermi surface at the doping level of interest is a hexagon inscribed within a hexagonal Brillouin zone (BZ), for both honeycomb and triangular lattices. The FS has three inequivalent corners, which are saddle points of the dispersion, marked by a vanishing Fermi velocity and a divergent density of states. The three inequivalent saddle points M_i are connected by three inequivalent nesting vectors $\mathbf{Q}_i$, each of which is equal to half a reciprocal lattice vector, such that $\mathbf{Q}_i = -\mathbf{Q}_i$. (b) Spin structure for the uniaxial SDW state. The SDW order quadruples the unit cell to a unit cell with eight sites (shaded). The enlarged unit cell has a large spin moment 3Δ on two sites and a small spin moment $-\Delta$ on the other six. The total spin on each unit cell is zero.

The model.—For definiteness, we focus on doped graphene at 3/8 filling. Our point of departure is the tight binding model [12], with the nearest-neighbor dispersion

$$\varepsilon_{\mathbf{k}} = -t_1\sqrt{1 + 4\cos\frac{k_y\sqrt{3}}{2}\cos\frac{3k_x}{2} + 4\cos^2\frac{k_y\sqrt{3}}{2}} - \mu, \quad (1)$$

where $\mu = -t_1$ at 3/8 filling. The FS then forms a perfect hexagon inscribed within a hexagonal BZ [Fig. 1(a)]. The perfect nesting of the FS in doped graphene is quite robust—it is broken only by third and higher neighbor hoppings, which are generally quite small. The Fermi velocity vanishes near the hexagon corners $\mathbf{M}_1 = (\pi/3, \pi/\sqrt{3})$, $\mathbf{M}_2 = (2\pi/3, 0)$, $\mathbf{M}_3 = (\pi/3, -\pi/\sqrt{3})$, which are saddle points of the dispersion:

$$\varepsilon_{\mathbf{M}_2+\mathbf{k}} \approx \frac{3t_1}{4}(k_y^2 - 3k_x^2),$$
$$\varepsilon_{\mathbf{M}_{1,3}+\mathbf{k}} \approx -\frac{3t_1}{4}2k_y(k_y \mp \sqrt{3}k_x), \quad (2)$$

where each time $\mathbf{k}$ denotes the deviation from a saddle point. Saddle points give rise to a logarithmic singularity in the DOS and control the SDW instability at weak coupling. There are three inequivalent nesting vectors connecting inequivalent pairs of saddle points [see Fig. 1(a)]:

$$\mathbf{Q}_2 = (0, 2\pi/\sqrt{3}), \qquad \mathbf{Q}_{1,3} = (\pm\pi/3, -\pi/\sqrt{3}). \quad (3)$$

Each $\mathbf{Q}_i$ is equivalent to $-\mathbf{Q}_i$, modulo a reciprocal lattice vector.

For the interactions, we use the low energy model from [7], which provides an exact description of the system in the weak coupling limit. This model contains four interactions: density-density, exchange, pair-hopping, and forward scattering, labeled g_1, g_2, g_3, g_4, respectively. Of these, the interactions g_4 and g_1 do not couple to spin density waves [7] and may be safely ignored [13]. The SDW physics is controlled by the density-density interaction g_2 ($|\mathbf{k}, \mathbf{k} + \mathbf{Q}_i\rangle \to |\mathbf{k}, \mathbf{k} + \mathbf{Q}_i\rangle$) and the umklapp pair-hopping interaction g_3 ($|\mathbf{k}, \mathbf{k}'\rangle \to |\mathbf{k} + \mathbf{Q}_i, \mathbf{k}' + \mathbf{Q}_i\rangle$). The partition function in the SDW sector can be written as $Z = \int D[\psi^\dagger, \psi]\exp(-S[\psi^\dagger, \psi])$, where $S = \int_0^{1/T} \mathcal{L}(\mathbf{k}, \tau)$ and

$$\mathcal{L} = \sum_\alpha \psi^\dagger_{a,\alpha}(\partial_\tau - \varepsilon_{\mathbf{k}} + \mu)\psi_{a,\alpha} - \sum_{\alpha\neq\beta} g_3 \psi^\dagger_{a,\alpha}\psi^\dagger_{a,\beta}\psi_{b,\beta}\psi_{b,\alpha} - g_2\psi^\dagger_{a,\alpha}\psi^\dagger_{b,\beta}\psi_{b,\beta}\psi_{a,\alpha}, \quad (4)$$

where the action is written in terms of electron operators, a, b are patch labels, and α and β are spin components.

Each nesting vector $\mathbf{Q}_i$ has associated with it an SDW order parameter $\mathbf{\Delta}_i = \mathbf{\Delta}_{a,b} = \frac{g_2+g_3}{3}\sum_k \langle \psi^\dagger_{a,\alpha}\boldsymbol{\sigma}_{\alpha\beta}\psi_{b,\beta}\rangle$. The condition for the emergence of each $\mathbf{\Delta}_i$ is the same: $((g_2 + g_3)/t_1)\log^2 t_1/T_N = O(1)$ [7], leaving a large number of SDW states as potential candidates. We study the selection of the SDW order within Ginzburg-Landau theory and by comparing different SDW solutions in the mean-field approximation for Eq. (4) at arbitrary $T < T_N$.

Ginzburg-Landau theory.—To construct the Ginzburg-Landau theory, we decouple the quartic interaction terms by restricting the interaction to the spin channel and a Hubbard-Stratonovich transformation to collective spin variables $\mathbf{\Delta}_i$. Note that the Hubbard Stratanovich transformation is exact and does not introduce any approximation. We integrate out the fermions in the Matsubara frequency representation and obtain an action in terms of $\mathbf{\Delta}_i$ in the form

$$\mathcal{L} = T\sum_{n=-\infty}^{\infty}\int\frac{d^2k}{(2\pi)^2}\Big[\frac{2}{g_2 + g_3}\sum_i(\mathbf{\Delta}_i)^2 + \mathrm{Tr}\,\ln\Big(i\omega_n - \varepsilon_{\mathbf{k}} - \sum_i \mathbf{\Delta}_i\cdot\boldsymbol{\sigma}\Big)\Big]. \quad (5)$$

For $T \approx T_N$, we can expand (5) in small $\mathbf{\Delta}_i/T_N$. It is useful to define the expansion coefficients

$$Z_i = T\sum_{\omega_n}\int\frac{d^2k}{(2\pi)^2}\xi_i, \quad (6)$$

where the integrands ξ_i are expressed in terms of fermionic Green functions $G = (i\omega_n - \varepsilon_{\mathbf{k}} - \mu)^{-1}$, $G_i = (i\omega_n - \varepsilon_{\mathbf{k}+\mathbf{Q}_i} - \mu)^{-1}$, and $G_{i+j} = (i\omega_n - \varepsilon_{\mathbf{k}+\mathbf{Q}_i+\mathbf{Q}_j} - \mu)^{-1}$ as

$$\xi_1 = G^2G_3^2, \qquad \xi_2 = G^2G_3G_1,$$
$$\xi_3 = GG_3G_1G_{1+3}, \qquad \xi_4 = G^2G_3^2G_1^2. \quad (7)$$

Diagrammatically, Z_1-Z_3 are given by "square" diagrams with four fermionic propagators and $\boldsymbol{\sigma}_{\alpha\beta}$ in the vertices, and Z_4 is given by a "hegagonal" diagram with six fermionic propagators, (see Fig. 2). The free energy evaluated at $T \approx T_N$ can be expressed in terms of these coefficients as

$$\mathcal{L} \propto \alpha(T - T_N)\sum_i \mathbf{\Delta}_i^2 + Z_1(\mathbf{\Delta}_1^2 + \mathbf{\Delta}_2^2 + \mathbf{\Delta}_3^2)^2 + 2(Z_2 - Z_1 - Z_3)(\mathbf{\Delta}_1^2\mathbf{\Delta}_2^2 + \mathbf{\Delta}_2^2\mathbf{\Delta}_3^2 + \mathbf{\Delta}_3^2\mathbf{\Delta}_1^2) + 4Z_3((\mathbf{\Delta}_1\cdot\mathbf{\Delta}_2)^2 + (\mathbf{\Delta}_2\cdot\mathbf{\Delta}_3)^2 + (\mathbf{\Delta}_3\cdot\mathbf{\Delta}_1)^2) - 4Z_4(\mathbf{\Delta}_1\cdot\mathbf{\Delta}_2\times\mathbf{\Delta}_3)^2 + \cdots \quad (8)$$

where α is an inessential positive constant.

The quadratic term and the first quartic term in (8) set the overall magnitude of $\Delta_{\mathrm{tot}}^2 = \sum_i \mathbf{\Delta}_i^2$ but do not differentiate between different SDW states. The second quartic term in (8) determines whether SDW order develops only at one nesting vector or at all three (depending on the sign of Z_2-Z_1-Z_3). Finally, the third quartic term and sixth order term control the relative orientation of the vector order parameters, if SDW order develops at multiple wave vectors. Close to T_N, the expansion to order $\mathbf{\Delta}_i^4$ is generally sufficient, but we include the sixth order term because Z_3 is suppressed by an extra factor of T_N/t_1, which is exponentially small in the weak coupling limit. The relative smallness of Z_3 arises because in the integrals for Z_1, Z_2, and Z_4, all fermions can be simultaneously brought to the saddle points, whereas in the integral for Z_3, three fermions can be

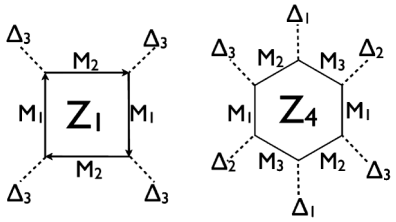

FIG. 2. The terms quartic in Δ are produced by processes represented diagrammatically by square diagrams. The diagrams for Z_2 and Z_3 correspond to patterns Δ_3, Δ_3, Δ_1, Δ_1 and Δ_3, Δ_1, Δ_3, Δ_1, respectively. The sixth order chirality sensitive term is produced by "hexagonal diagrams." Sample square and hexagonal diagrams are shown above. The integrals are dominated by momenta that bring all the fermion propagators to the vicinity of one of the saddle points of the dispersion.

brought simultaneously to saddle points, but the remaining fermion stays far away from the saddle point and the FS.

We evaluate the coefficients Z_1-Z_4 to leading order in small T_N/t_1 and obtain [13]

$$Z_1 = \frac{0.20 \log \frac{t_1}{T_N}}{\pi^4 T_c^2 t_1}, \qquad Z_2 = \frac{0.58}{\pi^4 T_N^2 t_1},$$
$$Z_3 = -\frac{0.08}{\pi^2 T_N^2 t_1}\frac{T_N}{t_1}, \qquad Z_4 = -\frac{0.1}{T_N^4 t_1}. \tag{9}$$

The positivity of Z_1 guarantees a second order phase transition, with the type of SDW order depending on the signs and relative magnitudes of Z_2, Z_3, and Z_4. Since Z_3 is smaller by T_N/t_1 than $Z_{1,2}$, and Z_2 is smaller by $\log\frac{t_1}{T_N}$ than Z_1, it follows that Z_2-Z_1-$Z_3 < 0$, so the system forms SDW order simultaneously at all three nesting vectors (the $3Q$ state). Meanwhile, the relative orientation of the three SDW order parameters is controlled by the sign of Z_3 at the smallest $\mathbf{\Delta}_i$, and by the sign of Z_4 at somewhat larger $\mathbf{\Delta}_i$. Both Z_3 and Z_4 are negative and favor the nonchiral SDW order with the three $\mathbf{\Delta}_i$ all aligned along the same axis.

An order parameter of the form $\mathbf{\Delta}(e^{i\mathbf{Q}_3\cdot\mathbf{r}} + e^{i\mathbf{Q}_1\cdot\mathbf{r}} \pm e^{i\mathbf{Q}_2\cdot\mathbf{r}})$ leads to spin moments on the lattice of the form shown in Fig. 1. A quarter of lattice sites have spin moment 3Δ, the other three quarters have moment $-\Delta$. Such an order cannot be obtained from any spin Hamiltonian for local moments of constant magnitude on every site. Our result differs from earlier mean-field analysis [11] which found noncoplanar insulating SDW order at weak coupling. We note, however, the $3Q$ state that we found, with nonequal spin length on different sites, was not considered in that work and other earlier considerations of SDW order. We found analogous results for fermions on a triangular lattice at van Hove filling, which are described by an identical low energy theory provided we neglect further neighbor hopping.

Properties of a uniaxial SDW.—Is the uniaxial SDW state a metal or an insulator? To address this issue we need to compute the fermionic spectrum. Without loss of generality, we take the SDW to be uniaxial along the z axis, so that S^z is a good quantum number, and spin-up and spin-down fermions decouple. Consider the state with $\mathbf{\Delta}_1 = \mathbf{\Delta}_2 = \mathbf{\Delta}_3 = \Delta\hat{\mathbf{z}}\sigma_3$. Up-spins near the three van Hove points are described by a simple Hamiltonian

$$H = \begin{pmatrix} \varepsilon_{1,\mathbf{k}} - \delta\mu & \Delta & \Delta \\ \Delta & \varepsilon_{2,\mathbf{k}} - \delta\mu & \Delta \\ \Delta & \Delta & \varepsilon_{3,\mathbf{k}} - \delta\mu \end{pmatrix}, \tag{10}$$

where ε_1, ε_2, ε_3 are the dispersions near the van Hove points, Eq. (2), and $\delta\mu$ is the SDW-induced shift of the chemical potential. The 3×3 Hamiltonian describing the spin-down branch is obtained by taking $\Delta \to -\Delta$. At $\mathbf{k} = 0$ (i.e., at van Hove points) the energies of spin-up excitations $E_\mathbf{k} - \delta\mu$ are $-\Delta$, $-\Delta$, and 2Δ, and the energies of spin-down excitations are Δ, Δ, and -2Δ. In conventional SDW states (e.g., SDW on a 2D square lattice), $\delta\mu/\Delta \propto T_N/E_F$ is negligibly small and can be safely neglected. We find that in our case $\delta\mu = -\Delta$, so that gapless excitations arise in the spin-down spectrum.

To see the unexpected shift of the chemical potential, we diagonalize Eq. (10) and the corresponding equation for down spins and inspect six branches of excitations. We find that fixing $\delta\mu = -\Delta$ ensures that both in the paramagnetic and in the $3Q$ uniaxial SDW state, there are four bands with $E_\mathbf{k} \le \mu$ and two bands with $E_\mathbf{k} \ge \mu$ for all momenta in the reduced BZ (see Fig. 3). Since the chemical potential is fixed by the constraint that the total number of electrons (equal to the number of states below the chemical potential) must not change between $\Delta = 0$ and $\Delta \neq 0$ [14], it follows that we must set $\delta\mu = -\Delta$. For verification, we computed the thermodynamic potential $\Omega(\Delta, \mu)$ from (5), numerically solved the simultaneous equations $\partial\Omega/\partial\Delta = 0$ and $\partial\Omega/\partial\mu = -N$, and confirmed that $\delta\mu = -\Delta$ to a high accuracy.

Having determined that $\delta\mu = -\Delta$, we find from (10) that gapless excitations emerge when $\varepsilon_{1,\mathbf{k}}\varepsilon_{2,\mathbf{k}}\varepsilon_{3,\mathbf{k}} = 0$, which has solutions along three lines passing through each van Hove point. Two of them coincide with the original FS; the third is directed towards the center of the BZ. The $3Q$ uniaxial SDW state is then obviously a metal. We emphasize, however, that gapless states exist only for the electrons with spin projection opposite to $\mathbf{\Delta}$. The electrons with spin projection along $\mathbf{\Delta}$ are fully gapped. Since a Fermi surface exists for one spin projection only, we dub this state a "half metal." We found an analogous "half-metal" spectrum for the $3Q$ uniaxial SDW phase on the triangular lattice.

The half-metallic nature of the SDW should manifest itself in numerous experiments. For example, in tunneling experiments conducted with electrons spin polarized along the z axis, a hard gap will be seen for down spins, but a Fermi surface will be seen for up spins. Furthermore, since the low energy charged excitations involve up spins only,

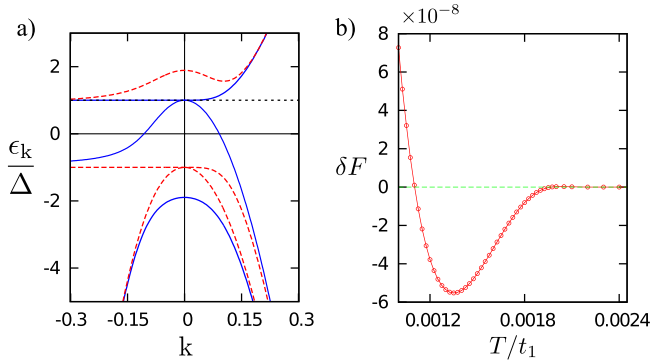

FIG. 3 (color online). (a) Excitation spectrum $\varepsilon_k = E_k - \delta\mu$ of the $3Q$ uniaxial state. Negative k are along the FS, positive k are along the BZ boundary in the original BZ (along k_x in the reduced zone). Placing the chemical potential at $\delta\mu = -\Delta$ ensures that four bands lie below the chemical potential (horizontal dotted line) and two lie above for all $\mathbf{k}$, irrespective of the value of Δ. Thus the choice $\mu = -\Delta$ conserves electron number. Excitations with spin projection opposite to $\mathbf{\Delta}$ are in blue (solid), along $\mathbf{\Delta}$ are in red (dashed) lines. Note that gapless excitations arise in the spin-down branch only. (b) Free energy difference $\delta F = F_{\text{uniaxial}} - F_{\text{chiral}}$ between the $3Q$ uniaxial SDW state and the chiral state, evaluated in the mean-field approximation for the honeycomb lattice Hubbard model with $g_2 = g_3 = U = 1.7t_1$ ($T_N \sim 0.002t_1$). The $3Q$ uniaxial state has lower Free energy over a wide range of intermediate temperatures, but at the smallest T the noncoplanar, chiral state, studied in earlier works [3,5,10], has lower Free energy.

any charge currents will necessarily also be spin currents. Thus, the half metal state allows for electrical control of spin currents, which may be beneficial for nanoscience applications.

Order parameter manifold.—The uniaxial SDW order obviously breaks $O(3)$ spin-rotational symmetry. It also breaks Z_4 discrete symmetry associated with either parallel or antiparallel ordering of $\mathbf{\Delta}_i$; i.e., in addition to the (Δ, Δ, Δ) state which we considered above, there are also (Δ, $-\Delta$, $-\Delta$), ($-\Delta$, Δ, $-\Delta$), and ($-\Delta$, $-\Delta$, Δ) states. These states have an identical structure of fermionic excitations and correspond to the four inequivalent ways to choose which two of the eight sites of the SDW unit cell carry large spins [see Fig. 1(b)]. Equivalently, the three other states from the Z_4 manifold are obtained from the (Δ, Δ, Δ) state by shifting the origin of coordinates to the center of one of three neighboring hexagons. An interesting possibility, which deserves further study, is that Z_4 symmetry can be broken before $O(3)$ symmetry, leading to a state of nematic type [15].

The phase diagram.—Thus far we have constructed the Ginzburg-Landau expansion in small Δ/T_N. This expansion becomes less justified as we move towards zero temperature. To investigate the behavior at arbitrary T, we calculate numerically the full Free energies of the various SDW states from (5). Upon doing this, we find that the $3Q$ uniaxial state has the lowest Free energy over a wide range of intermediate temperatures, roughly between $T_N/2$ and T_N, but undergoes a first order transition at a lower temperature to the insulating chiral SDW state discussed in earlier works [3,5,10]. We show the Free energy profile in Fig. 3(b). We found this behavior both for graphene and for fermions on a triangular lattice. Intuitively, the chiral SDW state wins at the lowest T because it has spin-degenerate excitations and opens a full spectral gap, unlike the half-metal state.

The Free energy profile in Fig. 3(b) is for weak or moderate coupling, when $T_N/t_1 \ll 1$. At $T_N \sim t_1$, the phase diagram is more complex. For completeness, we discuss the forms of Z_i and the phase diagram at $T_N \sim t_1$ in the Supplemental Material [13]. The ordering temperature T_N depends sensitively on the strength of the microscopic interactions. For graphene doped near the saddle point we estimate $T_N \approx$ 3–30 K, whereas $t_1 \approx 3$ eV [16]. Thus, at least for doped graphene, we should be decisively in the limit $T_N/t_1 \ll 1$, where our calculations apply.

Conclusion.—We considered in this Letter the SDW instability on the honeycomb and triangular lattices when doped to the saddle points of the dispersion. The SDW instability is subleading to a d-wave superconducting instability at weak coupling but becomes the leading instability if superconductivity is suppressed. We found that if the SDW ordering temperature T_N is much smaller than the fermionic bandwidth, then a uniaxial SDW order develops simultaneously at three inequivalent nesting vectors. This has an order parameter manifold $O(3) \times Z_4$ and corresponds to the ordering pattern shown in Fig. 1. Such a state can only be obtained from a model of itinerant electrons with interactions and not from a spin model of local moments. We found that such a SDW state is a half-metal in which gapless excitations exist in one spin branch only. Such a state may be beneficial for nanoscience applications particularly because charge currents will necessarily also be spin currents, which allows for electrical control of the latter.

We thank L. Levitov for numerous discussions concerning the interplay between superconductivity and SDW order. We are also thankful to C. Batista, R. Fernandes, I. Martin, and Fa Wang for useful conversations. G. W. C. is supported by ICAM and NSF-DMR-0844115, and A. V. C. is supported by NSF-DMR-0906953.

[1] A. H. Castro Neto, F. Guinea, N. M. R. Peres, K. S. Novoselov, and A. K. Geim, Rev. Mod. Phys. **81**, 109 (2009).
[2] J. L. McChesney, A. Bostwick, T. Ohta, T. Seyller, K. Horn, J. Gonzalez, and E. Rotenberg, Phys. Rev. Lett. **104**, 136803 (2010).
[3] T. Li, arXiv:1103.2420.
[4] D. Makogon, R. van Gelderen, R. Roldan, and C. M. Smith, Phys. Rev. B **84**, 125404 (2011).

[5] W. S. Wang, Y.-Y. Xiang, Q.-H. Wang, F. Wang, F. Yang, and D.-H. Lee, Phys. Rev. B **85**, 035414 (2012).
[6] B. Valenzuela and M. A. H. Vozmediano, New J. Phys. **10**, 113009 (2008).
[7] R. Nandkishore, L. Levitov, and A. Chubukov, Nature Phys. **8**, 158 (2012).
[8] M. Kiesel *et al.*, arXiv:1109.2953.
[9] J. Gonzalez, Phys. Rev. B **78**, 205431 (2008).
[10] I. Martin and C. D. Batista, Phys. Rev. Lett. **101**, 156402 (2008).
[11] T. Li, arXiv:1001.0620.
[12] P. R. Wallace, Phys. Rev. **71**, 622 (1947).
[13] See Supplemental Material at http://link.aps.org/supplemental/10.1103/PhysRevLett.108.227204 for details.
[14] B. Altshuler, A. V. Chubukov, A. Dashevskii, A. Finkelstein, and D. Morr, Europhys. Lett. **41**, 401 (1998).
[15] See, e.g., R. M. Fernandes, A. V. Chubukov, J. Knolle, I. Eremin, and J. Schmalian, Phys. Rev. B **85**, 024534 (2012) and references therein.
[16] In infinite 2D samples, $T_N = 0$, since $O(3)$ symmetry is restored by thermal fluctuations at any nonzero temperature in two dimensions. However, in a sample of finite size L, $T_N \approx T_{MF}/\log L/a$, where T_{MF} is the transition temperature neglecting thermal fluctuation effects, and a is the lattice scale. For samples of micron size, $\ln L/a \approx 7$, whereas T_{MF} was estimated in the supplement to Ref. [7] as 20–200 K. Thus, we arrive at our estimate $T_N \approx$ 3–30 K.